The behaviour of circular synthetic jets in a laminar boundary layer

S. Zhong, F. Millet, and N. J. Wood
School of Mechanical, Aerospace and Civil Engineering,
Manchester University, UK

ABSTRACT

Dye flow visualisation of circular synthetic jets was carried out in laminar boundary layers developing over a flat plate at a range of actuator operating conditions and freestream velocities of 0·05 and 0·1ms^{-1}. The purpose of this work was to study the interaction of synthetic jets with the boundary layer and the nature of vortical structures produced as a result of this interaction. The effects of Reynolds number (Re), velocity ratio (V_R) and Strouhal number (St) on the behaviour of synthetic jets were studied. At low Re and V_R, the vortical structures produced by synthetic jets appear as highly stretched hairpin vortices attached to the wall. At intermediate Re and V_R, these structures roll up into vortex rings which experience a considerable amount of tilting and stretching as they enter the boundary layer. These vortex rings will eventually propagate outside the boundary layer hence the influence of the synthetic jets on the near wall flow will be confined in the near field of the jet exit. At high Re and V_R, the vortex rings appear to experience a certain amount of tilting but no obvious stretching. They penetrate the edge of the boundary layer quickly, producing very limited impact on the near wall flow. Hence it is believed that the hairpin vortices produced at low Re and V_R are likely to be the desirable structures for effective flow separation control. In this paper, a vortex model was also described to explain the mechanism of vortex tilting.

1.0 INTRODUCTION

Synthetic jets are massless jets as they are formed from ambient fluids without net mass addition. A typical synthetic jet actuator consists of a cavity with rigid sidewalls, a rigid cap with a small orifice at one end and a vibrating diaphragm at the other as illustrated in Fig. 1. As the diaphragm vibrates the ambient fluid is drawn into and blown out of the orifice periodically, producing a jet made up of a train of vortical structures[1,2]. These vortical structures, if released into a boundary layer through its no-slip boundary, are capable of entraining faster moving fluids to the near wall region hence delaying flow separation.

There has been a strong research interest in synthetic jets since the late 1990s due to their potential application in flow control on aircraft[3-5]. Although it has been demonstrated in laboratory experiments that synthetic jets are capable of improving the performance of lift-producing bodies by delaying flow separation[6,7], their detailed fluid mechanics is still far from fully understood.

The research on synthetic jet actuators has been carried out at the Goldstein Aeronautical Laboratory at Manchester University since 1998. Smoke visualisation studies of synthetic jets in quiescent conditions has led to an improved understanding of the influence of cavity and orifice geometry on the behaviour of synthetic jets that would be beneficial to actuator design[8]. The flow control effectiveness of an array of synthetic jet actuators has been tested by implementing them beneath the surface of a circular cylinder upstream to its separation line at a Reynolds number based on the cylinder diameter of $5{\cdot}5 \times 10^5$ [9,10]. A turbulent boundary layer was generated using a trip wire mounted near the leading edge of the cylinder. Surface oil flow patterns revealed that with the actuators active the separation line was pushed downstream considerably. In particular, the oil flow revealed the footprints of a well-defined streamwise vortex pair immediately downstream of each synthetic jet (see Fig. 2). These vortex pairs appeared to persist for a long distance downstream and interact with the separated flow resulting in a delayed separation. In order to understand how the vortex rings which formed the synthetic jets produced these interesting structures, Crook *et al* conducted a series of dye flow visualisation experiments to study the behaviour of synthetic jets under the influence of a crossflow[11]. Under certain test conditions in their experiments, vortex rings produced by synthetic jets were tilted to a high extent and stretched as they entered the flow field. Crook *et al* hypothesised that those determinant streamwise

Paper No. 2980 Received on 26 April 2005, accepted 13 July 2005.

https://doi.org/10.1017/S0001924000000877 Published online by Cambridge University Press

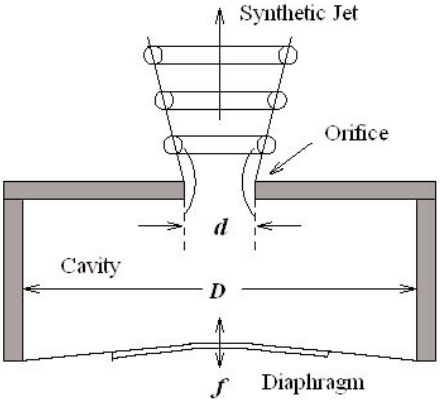


Figure 1. Schematic diagram of a synthetic jet produced with an oscillating diaphragm.

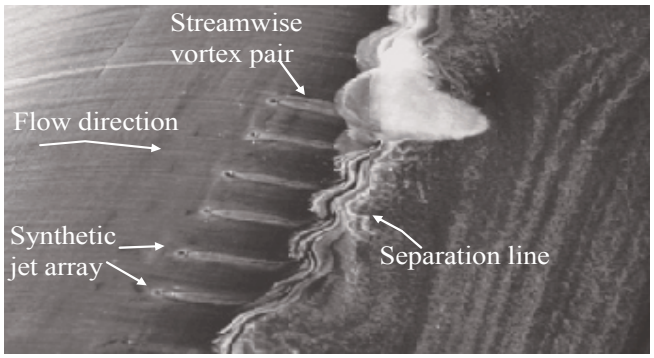


Figure 2. Oil flow pattern on the circular cylinder model showing the streamwise vortex pairs produced by a spanwise array of synthetic jets[11]. The diameter of the synthetic jet orifice is 1mm. The diameter of the cylinder is 0·27m.

structures revealed by oil flow on the surface of the circular cylinder model were produced by agglomeration of tilted and highly stretched vortex rings.

Following on from the aforementioned investigation in crossflow, the present work considers a boundary-layer flow in order to further examine the mechanism by which the streamwise structures were produced. It aims to study the interaction of synthetic jets with the boundary layer, investigate the nature of vortical structures produced as a result of this interaction and identify the type of structures which are potentially more effective in delaying flow separation. It was observed in the initial dye visualisation experiments that the vortical structures produced by synthetic jets were essentially similar in both laminar and turbulent boundary layers upon changes in actuator operating conditions and freestream conditions. Hence to simplify the interpretation of results, the present experiments were undertaken in a laminar boundary layer.

2.0 EXPERIMENTAL SET UP

The dye flow visualisation experiments were performed in a tilting flume at the Goldstein Laboratory at Manchester University. The test section of the flume is 4m in length and has a cross-sectional area of 0·3m × 0·3m. The maximum freestream velocity in the test section is approximately 0·2ms^{-1}.

The test model was made of an aluminum plate 1·1m long, 0·3m wide and 6mm thick, mounted at a fixed height parallel to the test section floor. It has a sharp leading edge and was tilted at a very small negative incidence to the incoming flow. This arrangement effectively eliminates flow separation at the leading edge and ensures that a laminar boundary layer forms at the leading edge of the plate.

The synthetic jet actuator has a cylindrical cavity of D = 100mm in diameter and 20mm in height. The cavity orifice has a diameter of d = 5mm and a depth of 6mm. The synthetic jet was produced by an oscillating diaphragm that was clamped around its edge at the end of the cavity. The diaphragm was attached to a magnetic shaker via a steel rod which was driven with sinusoidal signals of chosen frequencies and amplitudes. The amplitudes of the diaphragm oscillation were measured with an eddy-current displacement sensor.

The orifice of the cavity was located at 0·72m aft the leading edge of the test plate. The freestream velocity was measured with a propeller-type stream probe. Typical boundary-layer thickness at the location of the orifice opening was approximately 15mm at the test conditions, giving a boundary layer thickness to the orifice diameter ratio δ/d of about 3. The flow conditions for all the tests are listed in Table 1. Here θ is the momentum thickness of the local boundary layer.

Since the shaker must be isolated from water, the plate was mounted with its test surface facing downwards as shown in Fig. 3. Dye was introduced to the cavity by gravity. In the experiments, the dye pattern produced by synthetic jets was recorded on tapes using a digital video camera. Most of the images were recorded from a view through the side window of the test section. As the floor of the flume was made of solid metal, plan-view of the synthetic jets was not available. Hence in order to obtain a three-dimensional impression of these jets, some images were also taken at an oblique angle below the test surface from an upstream point of view.

3.0 NON-DIMENSIONAL FLOW PARAMETERS

In the present experiments, the geometry of the synthetic jet actuator was fixed. The characteristics of the jets were varied by changing the diaphragm operating conditions (oscillation frequency and amplitude) and the freestream velocity. For synthetic jets in a uniform cross flow, it has been established that their behaviour is dictated by three non-dimensional flow parameters, i.e. the Reynolds number, the velocity ratio and the Strouhal number[10]. For synthetic jets that are released into a laminar boundary layer, they are also expected to be affected by the relative size of the boundary layer thickness to the

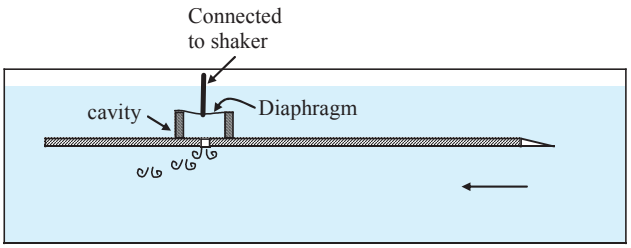


Figure 3. Schematic sketch of the test section.

Table 1
Flow conditions

U_∞ (ms^{-1})	Re_θ	δ/d
0·05	394	3·7
0·10	547	2·7

https://doi.org/10.1017/S0001924000000877 Published online by Cambridge University Press

orifice diameter as well as the level of shear in the boundary layer.

In this study, the Reynolds number is defined as

$$\mathrm{Re} = \frac{\bar{U}_0 L_0}{v} \quad \ldots (1)$$

where v is the kinematic viscosity of the fluid. $\bar{U}_0$ is the time-averaged velocity over the blowing cycle of the synthetic jet actuator at the exit of the orifice and can be calculated as

$$\bar{U}_0 = \frac{1}{T}\int_0^{T/2} \tilde{u}_0(t)\mathrm{d}t \quad \ldots (2)$$

if the space-averaged velocity at the exit $\tilde{u}_0(t)$ is known. The stroke length L_0 is equivalent to the length of a cylindrical slug of diameter d which contains the mass flow expelled during the blowing cycle and it is related to $\bar{U}_0$ via

$$L_0 = \bar{U}_0 T \quad \ldots (3)$$

where f is the vibration frequency of the diaphragm. Being proportional to the total circulation ejected during the blowing cycle of the synthetic jet[2, 12], the Reynolds number based on the stroke length (Eq. 1) is believed to be a good indicator of the strength of the vortex ring.

The velocity ratio V_R is commonly used to represent the relative strength between the jet and the crossflow. In the present experiment, it is defined as the ratio between the time-averaged velocity $\bar{U}_0$ and the freestream velocity U_∞.

$$V_R = \frac{\bar{U}_0}{U_\infty} \quad \ldots (4)$$

The Strouhal number can be defined as

$$St = \frac{fd}{U_\infty} \quad \ldots (5)$$

The use of U_∞ instead of $\bar{U}_0$ in defining the Strouhal number emphasizes the influence of the freestream flow on the periodic behaviour of the synthetic jet. In the authors' opinion, the Strouhal number based on $\bar{U}_0$ is more appropriate for synthetic jets produced in a quiescent flow where the vortex rings propagate away from the orifice under the combined influence of the jet flow and their self-induced velocity. This Strouhal number gives an indication of the spacing between consecutive vortex rings in quiescent flow and the extent of influence that the suction cycle has on the formation of the synthetic jet. When an external flow is present, the vortex rings will be forced to convect with that flow shortly after they emerge from the orifice. Hence in this case the periodical nature of the jet is expected to be strongly affected by the external flow and the use of the Strouhal number based on U_∞ would be more appropriate in describing the behaviour of synthetic jets in a cross flow or a boundary layer.

Since the ratio between the boundary layer thickness and orifice diameter only varied within a small range (from 2·7 to 3·7) in the present experiment, it is considered to have a secondary effect on the results. Considering the importance of shear in the boundary layer on the behaviour of synthetic jets, one may tentatively introduce the ratio between the jet velocity and friction velocity $\bar{U}_0/U_\tau$ to account for the influence of shear. Nevertheless, in the present experiment U_τ/U_∞ varies insignificantly (from 0·024 to 0·020) when the freestream velocity is doubled. Hence the velocity ratio defined in Eq. (4) is equivalent to $\bar{U}_0/U_\tau$ in an approximate sense. As the first study in a series, the present study will focus on the effect of changing Reynolds number, velocity ratio and Strouhal number on the behaviour of synthetic jets. This work will provide a foundation for a further investigation on the effect of changing boundary layer thickness to orifice diameter ratio and level of shear in the boundary layer.

Because the jet velocity is not measured in the present experiments, the time-averaged velocity at the orifice exit was estimated using the following relation

$$\bar{U}_0 = \frac{1}{4} f \Delta \left(\frac{D}{d}\right)^2 \quad \ldots (6)$$

where Δ is the peak-to-peak displacement at the centre of the diaphragm. This formula clearly shows that the jet time-averaged velocity is proportional to the product of diaphragm vibration frequency and amplitude for a given actuator. Equation (6) was derived by Tang and Zhong[13] by equating the instantaneous volume flow rate displaced by the diaphragm to that expelled through the orifice. The instantaneous shape of the diaphragm was calculated using the theory of thin shell assuming the edge of the diaphragm is clamped. The velocity predicted with this equation was found to be in good agreement with the measurements made on incompressible synthetic jets in a quiescent flow[14]. Examination of the vertical distance that the vortex ring moves between consecutive frames near the exit of the orifice shows that the agreement in the present case, where a boundary layer is present, is also reasonable. Hence this formula is considered useful in estimating the values of non-dimensional parameters for the purpose of comparing the characteristics of synthetic jets produced at different flow and actuator operating conditions.

In this experiment, dye visualisation of synthetic jets were carried out with diaphragm peak-to-peak displacements ranging from 0·028 to 0·07mm and frequencies from 2 to 5Hz at freestream velocities of U_∞ = 0·05 and 0·1ms^{-1}. The corresponding range of Re was from 16 to 245, V_R from 0·06 to 0·7 and St from 0·1 to 0·5. The stroke length normalised by the orifice diameter ranged from 0·56 to 1·4. The lowest diaphragm oscillation frequency was at least four times higher than that of the Tollmien-Schlichting waves that may be encountered in the boundary layer. Hence the stability of the boundary layer is not expected to be affected by the synthetic jets.

4.0 RESULTS AND DISCUSSION

4.1 Vortical structures produced by synthetic jets

Figure 4 shows a close-up view of the vortical structures that emerge from the orifice at a number of diaphragm oscillation frequencies and amplitudes at a freestream velocity of U_∞ = 0·05ms^{-1}. Although the images were not taken at the same phase during the diaphragm oscillating cycle but instead at an arbitrary instant when the structure fully emerged from the orifice, they still enable the nature of the vortical structure produced at different conditions to be compared.

Since the freestream velocity is fixed in this case, a rise in the velocity ratio or the Reynolds number is caused by an increase in the jet velocity due to an increase in either the diaphragm oscillation frequency or displacement whereas an increase in Strouhal number is the result of an increase in diaphragm oscillation frequency only. It can be seen that over the range of Strouhal numbers examined in this case ($0{\cdot}2 \le St \le 0{\cdot}5$), the vortical structure rolls up into a vortex ring at Re ≥ 35 and $V_R \ge 0{\cdot}17$. As the Reynolds number and velocity ratio increases, the circulation in the ring also increases, which corresponds to larger vortex rollers. At the two lowest Reynolds number and velocity ratio settings (Re = 16 and 24, V_R = 0·11 and 0·17), no roll-up occurs on the upstream side of

https://doi.org/10.1017/S0001924000000877 Published online by Cambridge University Press

the orifice, and hence an asymmetrical vortical structure is produced (see Fig. 4(a) and 4(d)). Although the structure formed at Re = 31 and V_R = 0·21 (Fig. 4(g)) appears to be asymmetric also, it turns out to be a vortex ring in Fig. 6(g).

At a given freesteam velocity, the velocity ratio increases along with the Reynolds number as the jet velocity increases. Hence it is not possible to separate the effect of these two non-dimensional parameters by examining the results obtained at one freestream velocity alone. For the images shown in Fig. 5, the freestream velocity is doubled resulting in *St* and V_R being halved whereas Re remains unchanged at the same diaphragm frequencies and amplitudes. Despite the differences in *St* and V_R, it is noted that the two distinct patterns seen in Fig. 4 are observed at a similar range of Reynolds numbers. In addition, the strength of vortex rings is again found to be strongly correlated to the magnitude of the Reynolds number. The latter confirms that the use of the Reynolds number based on the stroke length is appropriate in quantifying the strength of vortex rings. If the orifice diameter were used as the length scale, cases which obviously show vortex rings of different vorticity strengths such as those seen in Fig. 4(b) and 4(d) will be labelled with the same Reynolds number. At a given freestream condition, the circulation of the vortex ring decreases as the jet velocity reduces. It is likely that at the two lowest Reynolds numbers (Re = 16 and 24), the upstream branch of the vortex ring is significantly suppressed by the resident vorticity in the boundary layer and is subsequently drawn into the orifice at the onset of the suction cycle, resulting in an asymmetric structure as shown in Fig. 4(a), 4(d), Fig. 5(a) and 5(d).

It is found that at both freestream velocities asymmetric roll-up occurs at the same Reynolds number (see Fig. 4(a), 4(d), Fig. 5(a) and 5(d)). Based on the experimental observations presented here, it seems that the onset of an asymmetric roll-up depends on the Reynolds number, which determines the level of circulation in the vortex ring. It is believed, however, that the vortex roll-up at the exit of the orifice will also be affected by other factors, such as the strength of the resident vorticity in the boundary layer and how far the structure has moved away from the orifice when the suction cycle starts. More experiments covering a wider range of the non-dimensional parameters will be needed to further this investigation.

The velocity ratio gives an indication of the relative strength between the jet and incoming flow in terms of velocity. The circulation in the upstream branch of the vortex ring produces a tangential velocity which is in the opposite direction to the local velocity in the boundary layer. It is observed that at U_∞ = 0·1ms^{-1} and at a relatively low Reynolds number the upstream branch of the ring tends to be blown towards the downstream side of the ring (see Fig. 5(b) and 5(c)). This kind of impact is so severe that at lower Reynolds numbers the upstream branch appears to wrap around the downstream branch (see Fig. 5(g) and 5(j)). However at U_∞ = 0·05ms^{-1}, the vortex rings are less affected since their strength relative to the incoming flow increases (see Fig. 4(b), 4(c) and 4(j)).

4.2 Interaction between vortical structures and the boundary layer

In order to investigate the behaviour of the synthetic jets in the boundary layer, image sequences of vortical structures as they enter the layer and propagate downstream are examined. Snap shots of a train of these structures generated at the same diaphragm operating conditions and freestream velocity as for Fig. 4 are shown in Fig. 6. At Re = 16 and V_R = 0·11 there is no roll-up of vortex rings and the structures produced by the synthetic jets appear as elongated vortices, which stem from the wall and are inclined downstream in the boundary layer (see Fig. 6(a)). As the diaphragm displacement increases (Re = 24, V_R = 0·17), the synthetic jets roll up into vortex rings which undergo subsequent tilting and stretching as they migrate across the boundary layer and propagate downstream (see Fig 6(b)). Further increase in diaphragm displacement results in turbulent vortex rings which penetrate the edge of the boundary layer within a short distance (see Fig 6(c)). Similar trend with varying diaphragm displacements was observed at higher diaphragm frequencies except that, due to the higher jet velocity, the trajectory of the vortical structures at a higher frequency is steeper (see Fig. 6(d)-(f)) and the onset of a full vortex roll-up tends to occur at a lower diaphragm displacement (see Fig. 6(g)).

Snap shots of a train of vortical structures generated at the same diaphragm operating conditions at U_∞ = 0·1ms^{-1} as for Fig. 5(a)-(i) are shown in Fig. 7. Similar changes in the patterns of flow structures with increasing diaphragm displacements at a given frequency that were seen at U_∞ = 0·05ms^{-1} are also observed. Again, in most cases vortex ring like structures are observed (see Fig. 7(c), (e), (f) and (g)-(i)). The structures seen in Fig. 7(a) and 7(d) are similar to those observed in Fig. 6(a) and 6(d). At the same frequency and displacement, an increase in freestream velocity results in the structures remaining closer to the wall and separating further apart from each other (compare Fig. 6(b) with Fig. 7(b)). Furthermore at the same Reynolds number the flow structure appears more diffused due to the impact of the incoming flow with a higher velocity. This makes the dye patterns less well defined, especially at low diaphragm amplitudes.

To understand the effect of an individual non-dimensional parameter has on the behaviour of synthetic jets, comparisons are made by varying only one of the three non-dimensional parameters each time using a selected combination of diaphragm operating conditions and freestream velocities. Although the number of matching cases is limited, some useful information can still be obtained. At the same *St* and V_R, an increase in Re does not seem to affect the trajectory but produces stronger vortex rings, which are more capable of resisting the resident vorticity in the near wall boundary layer such that they tend to have a stronger upstream branch (compare Fig. 6(a)-(c) with Fig. 7(h)-(i)). In particular, a full vortex roll up occurs at Re = 31 whereas the roll up only occurs at the downstream side at Re = 16 (compare Fig. 4(a) and Fig. 5(g)). It appears that the Strouhal number affects the spacing between consecutive structures. At the same Strouhal number the average spacing between consecutive structures appears to be the same despite the differences in the Reynolds number (compare Fig. 6(a)-(c) with Fig. 7(h)-(i)). In addition, the spacing decreases as the Strouhal number increases and as a result the tendency of interaction between neighbouring vortices should increase, especially at high diaphragm oscillation frequencies (compare Fig. 6(b) with 7(b), Fig. 6(e) with 7(e)). The matching cases for assessing the effect of V_R are not available, but assuming the Strouhal number mainly affect the spacing between consecutive structures, a comparison between images acquired at the same Reynolds number but different V_R can still be useful. It is found that a larger V_R produces a steeper vortex ring trajectory due to an increase in the jet velocity relative to the freestream (compare Fig. 6(i) with 7(i)).

To provide further information about the nature of the structures produced by synthetic jets, video images were also taken from an oblique view underneath the plate from an upstream location. For convenience of comparison, the side-view of the structures shown in Fig. 6(a)-(c) is presented again in Fig. 8(a)-(c). It appears in Fig. 9(a) that the elongated structures seen in Fig. 8(a) are in fact hairpin vortices which are highly stretched by the shear in the near wall region. The same observation also applies to the cases shown in Fig. 7(a) and 7(d). In the case shown in Fig. 8(b), vortex rings are formed. Due to the interaction between the vortex ring and the boundary layer, the vorticity in the downstream part of the ring becomes intensified whereas that in the upstream part is weakened by the resident vorticity in the boundary layer (Fig. 9(b)). Although the upstream part of the structure appears to be missing at a later time giving an initial impression of a horseshoe vortex, it is believed that the structure remains as a vortex ring. It is most likely that the upstream part of the ring becomes too weak to entrain sufficient amount of dye to make itself visible. The fact that these structures continuously propagate

https://doi.org/10.1017/S0001924000000877 Published online by Cambridge University Press

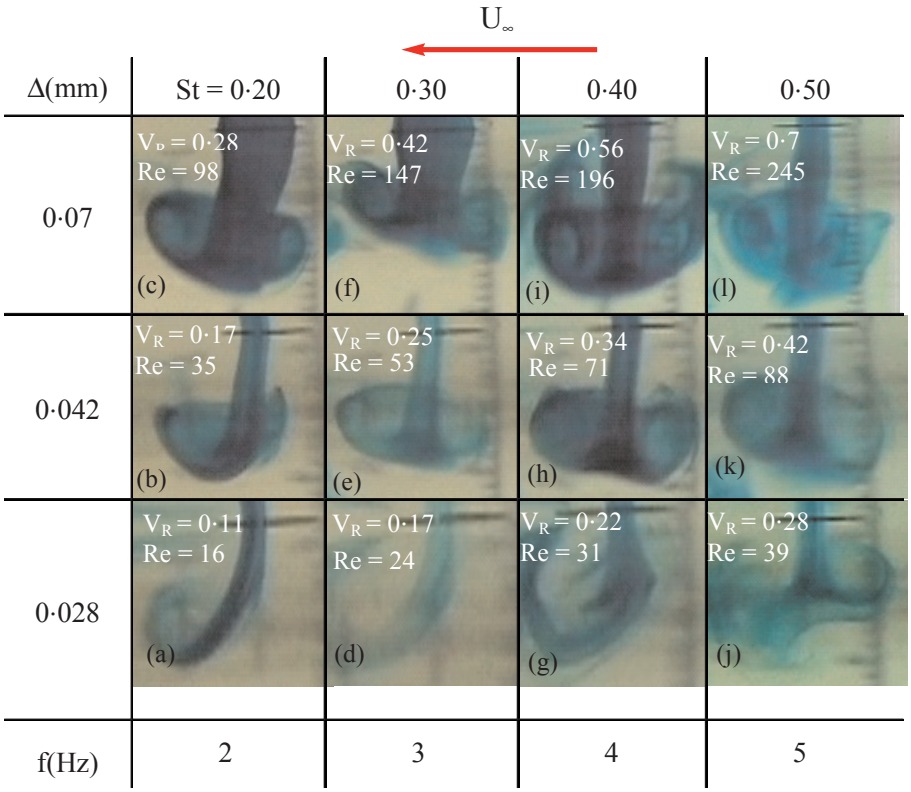


Figure 4. Close-up view of synthetic jets produced with different diaphragm displacements and frequencies in a laminar boundary layer at $U_\infty = 0{\cdot}05 ms^{-1}$.

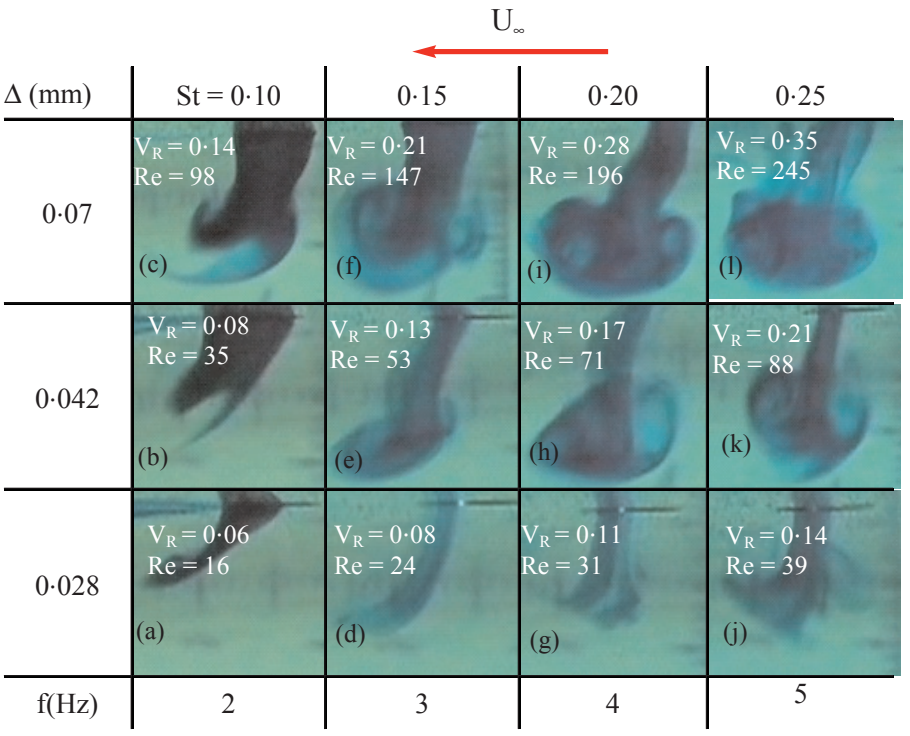


Figure 5. Close-up view of synthetic jets produced with different diaphragm displacements and frequencies in a laminar boundary layer at $U_\infty = 0{\cdot}1 ms^{-1}$.

https://doi.org/10.1017/S0001924000000877 Published online by Cambridge University Press

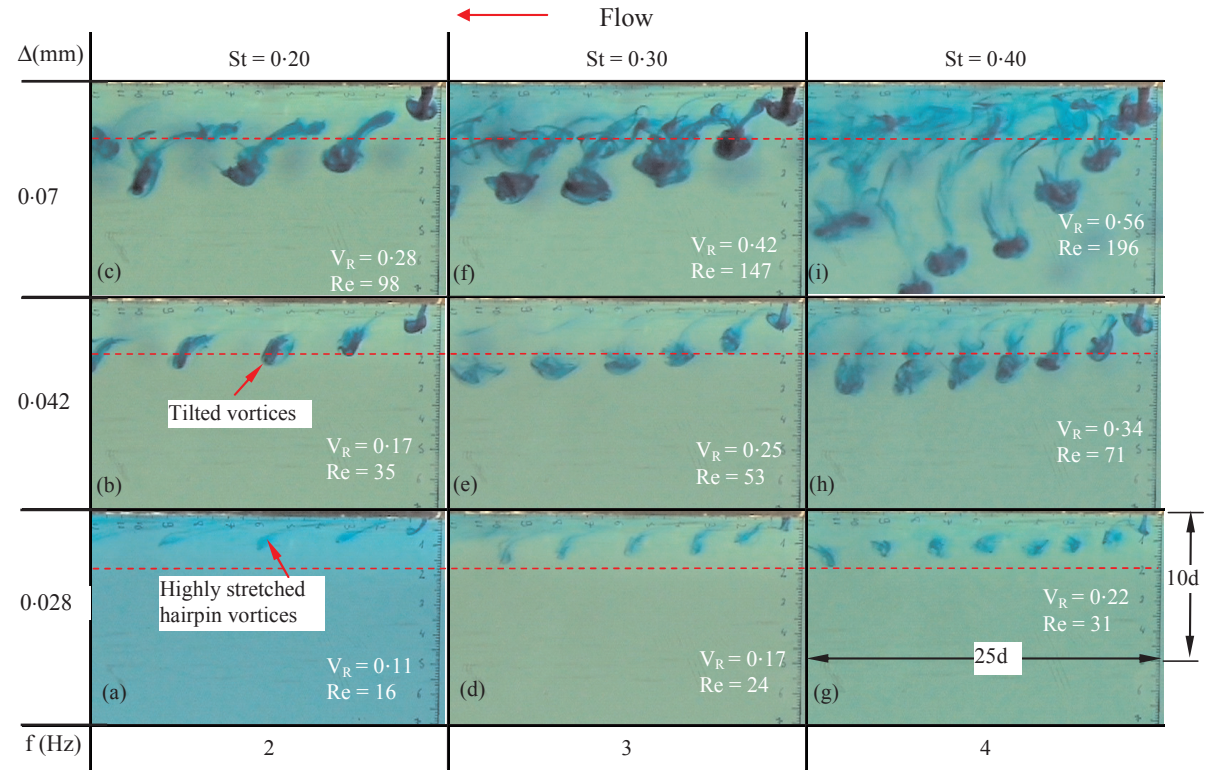


Figure 6. Side-view of vortical structures produced by synthetic jets at U_∞ = 0·05ms^{-1}. Dash line indicates the edge of the laminar boundary layer. The scales shown in the background are in cm.

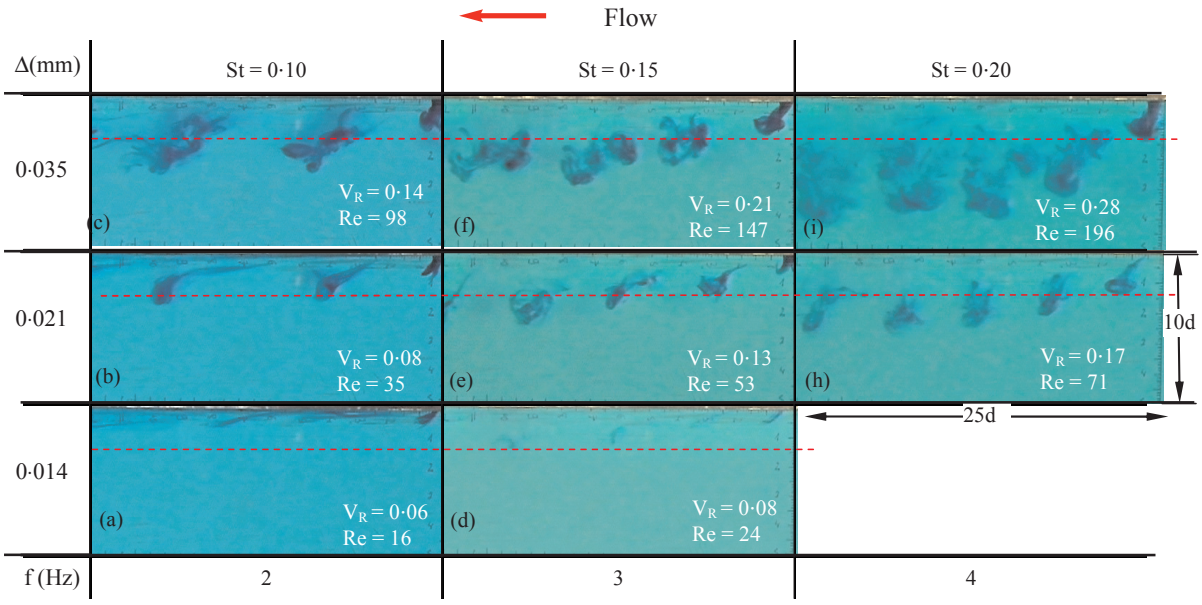


Figure 7. Side-view of vortical structures produced by synthetic jets at U_∞ = 0·10ms^{-1}. Dash line indicates the edge of the laminar boundary layer. The scales shown in the background are in cm.

https://doi.org/10.1017/S0001924000000877 Published online by Cambridge University Press

away from the wall, suggests that they are not bounded to the wall as the horseshoe vortices. The rearrangement of vorticity strength in the upstream and downstream branches of the vortex ring tends to be observed at moderate Reynolds number when the vortex rings are subject to significant influence of shear in the boundary layer due to their relatively long resident time in the layer. In this case, the impact of vortex rings on the near wall flow may be confined within a certain distance downstream of the orifice before they propagate away from the boundary layer. It is seen that as the diaphragm displacement increases further, the vortex rings become distorted and penetrate the boundary layer quickly, leaving little trace in the near wall region (Fig. 8(c) and 9(c)).

It is also worth examining the structures seen in Fig. 8(d) in further detail. In this case, there is a weak roll-up at the upstream side of the orifice and the weak upstream branch is blown towards the downstream branch by the incoming flow. However, since the strength of the vorticity in the upstream branch is insufficient to counteract against the resident vorticity of the opposite sign in the incoming boundary layer, it quickly becomes diffused leaving only the downstream branch which forms a hairpin-like structure. The structure observed in Fig. 8(d) may be regarded as an intermediate case between the cases shown in Fig 8(a) and 8(b). This observation also applies to what is seen in Fig. 6(d).

Based on the above observation, it is seen that only the vortcial structures which appear as hairpin vortices will remain in the boundary layer with their legs trailing along the wall for a significant distance. In the cases where synthetic jets emerge from the orifice as strong vortex rings, the rings will eventually penetrate the boundary layer under the continuous influence of their self-induced velocity producing limited impact on the flow in the near wall region. Hence it is likely that the persistent streamwise structures observed by Crook *et al* on the cylinder model[9,10] were produced by the overlapping legs of hairpin vortices rather than agglomeration of tilted and highly stretched vortex rings. These hairpin vortices could be the desirable vortical structures required for effective flow control with minimal power consumption. Further evidence confirming this conjecture will be sought by conducting detailed velocity measurements of synthetic jets in the boundary layer.

4.3 Vortex stretching and tilting mechanism

In the present studies, vortex stretching and tilting are the key features observed in the dynamic behaviour of the vortical structures produced by synthetic jets. Vortex stretching of different extents is present for all the cases whereas vortex tilting only occurs when vortex rings are formed.

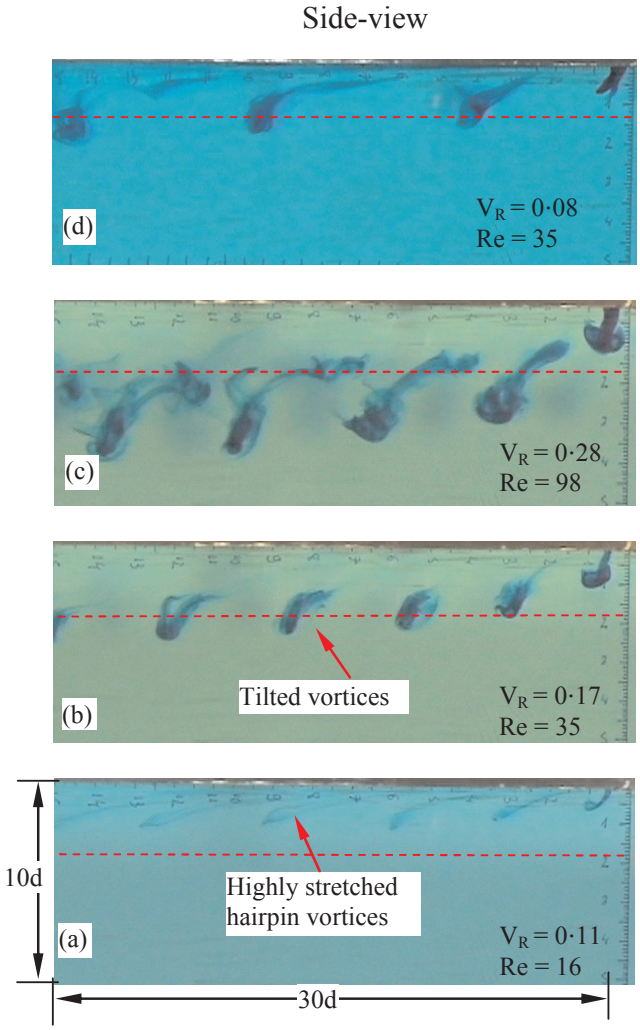


Figure 8. Side-view of vortical structures produced by synthetic jets at U_∞ = 0·05ms^{-1} and f = 2Hz, (a). Δ =0·028mm, (b). Δ =0·042mm, (c). Δ = 0·07mm, and (d). U_∞ =0·1ms^{-1} and f = 2Hz, Δ =0·042mm.

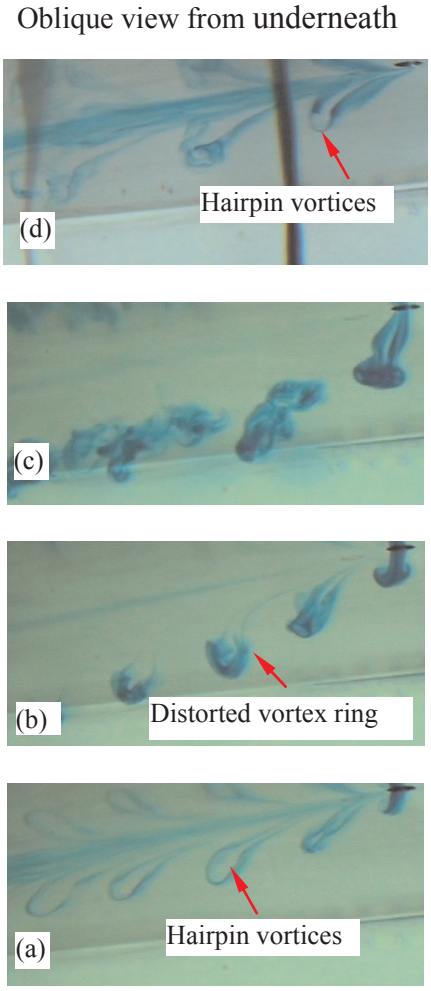


Figure 9. Oblique view of vortical structures produced by synthetic jets at conditions identical to those in Fig. 8.

https://doi.org/10.1017/S0001924000000877 Published online by Cambridge University Press

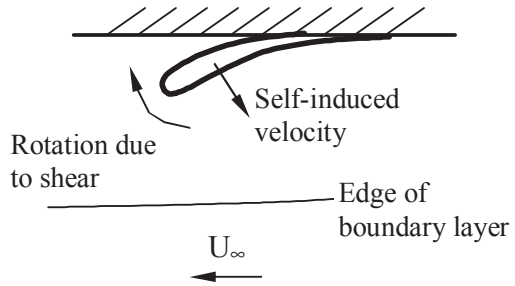


Figure 10. Hairpin vortex at a characteristic inclination angle to the wall under the opposing effects of self-induced velocity and shear.

At low Reynolds numbers and velocity ratios (Re ≤ 24 and V_R ≤ 0·17), vortex stretching is predominant. In these cases the vortex roll-up is asymmetric with the upstream branch of the vortex ring being suppressed and the vortical structure produced by synthetic jets appears in the form of hairpin vortices with their legs attached to the wall. These vortices are highly stretched under the influence of shear in the boundary layer. Eventually they will be inclined at an angle to the wall under the opposing effects of self-induced velocity that peels the vortices away from the wall and the shear in the boundary layer that rotates them back to the wall as illustrated in Fig 10. In this case, vortex stretching enhances the vorticity in the hairpin vortices and hence allows the induced velocity to be maintained or even increased to counteract against dissipation. As suggested by the study carried out by Head and Bandyopadhyay on hairpin vortices in fully turbulent boundary layers[15], the inclination angle of hairpin vortices is likely to be between 45° and 60° with the rate of stretching reaching its maximum at 45°. Here the inclination angle of hairpin vortices produced by synthetic jets seems to correlate with their hypothesis (Fig. 10).

At high Reynolds numbers and velocity ratios (Re ≥ 71 and V_R ≥ 0·28), the synthetic jets roll up into vortex rings which experience a certain amount of tilting but no obvious stretching as they move away from the wall and downstream. The rings penetrate the edge of the boundary layer quickly, producing very limited impact on the near wall flow.

Vortex tilting and stretching are more dramatic at intermediate Reynolds numbers and velocity ratios (see Fig. 11). At time zero, a slug of fluid emerges from the orifice (Fig. 11(a)) which subsequently rolls up into a vortex ring (Fig. 11(b)). Initially the two sides of the vortex ring are roughly parallel to the wall. However, it experiences a steady anti-clockwise tilt soon after and at the same time the vortex ring is also stretched under the influence of shear in the boundary layer (Fig. 11(d)-(f)). The suction cycle of the synthetic jet starts between the instants corresponding to Fig. 11(c) and 11(d). It appears that the start of tilting is coupled with the onset of the suction cycle which subsequently pulls the upstream part of the vortex ring towards the wall as it convects over the orifice. As the vortex ring propagates further away from the orifice, it continues to tilt before it finally reaches a constant angle to the wall. This is supported by the difference in the orientation between the downstream and the upstream vortex rings seen in Fig. 11(f).

Similar phenomenon was also observed by Crook *et al* in their cross flow experiment[11] in which the ratio of the orifice diameter to the local boundary-layer thickness was approximately one. They suspected that the onset of suction cycle played an important role in causing the vortex ring to tilt. In the present experiment, the boundary layer thickness was much greater than the orifice diameter allowing a closer examination of the tilting process. The fact that tilting continues even after the vortex ring has moved sufficiently far away from the orifice indicates that another mechanism is present.

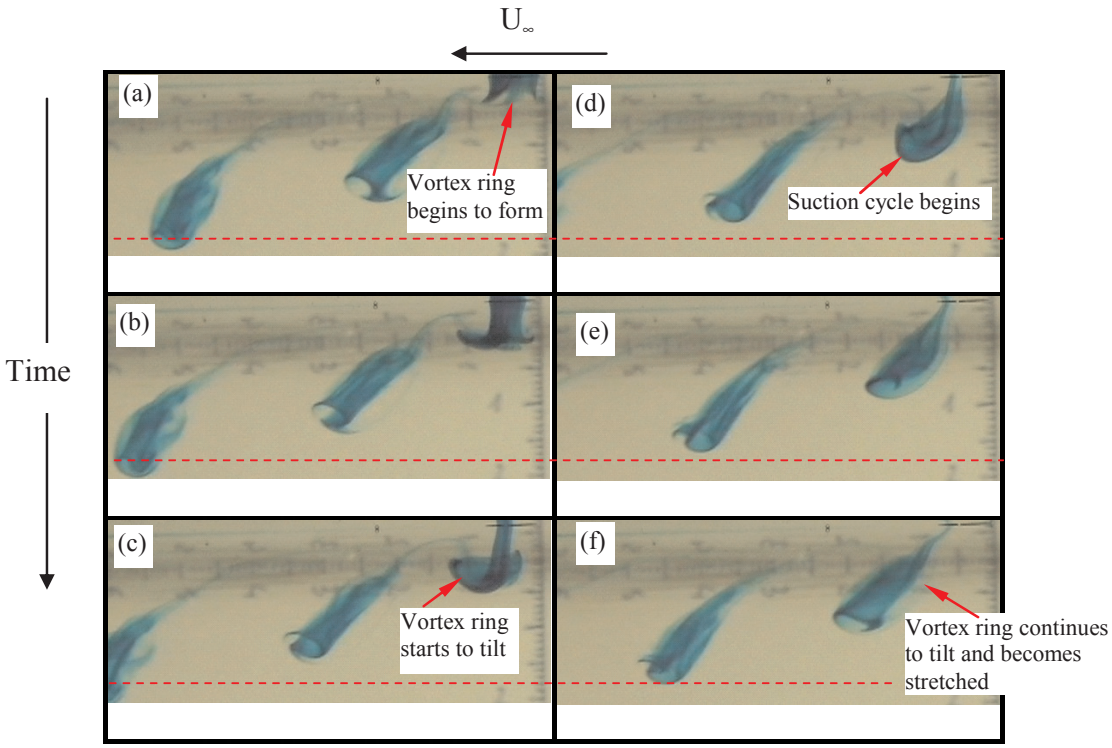


Figure 11. Sequence of images illustrating the process of vortex tilting, U_∞ = 0·05ms^{-1}, f = 2Hz, Δ = 0·042mm (Re = 35, St = 0·2, V_R = 0·17).

https://doi.org/10.1017/S0001924000000877 Published online by Cambridge University Press

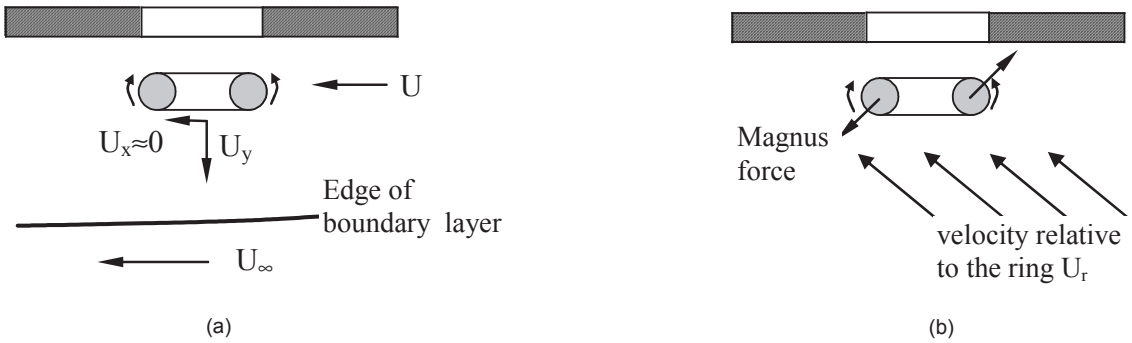


Figure 12. A vortex ring as it emerges from the orifice
(a) Its velocity components in a stationary coordinate. (b) Flow velocity relative to the ring and the Magnus forces acting on the ring.

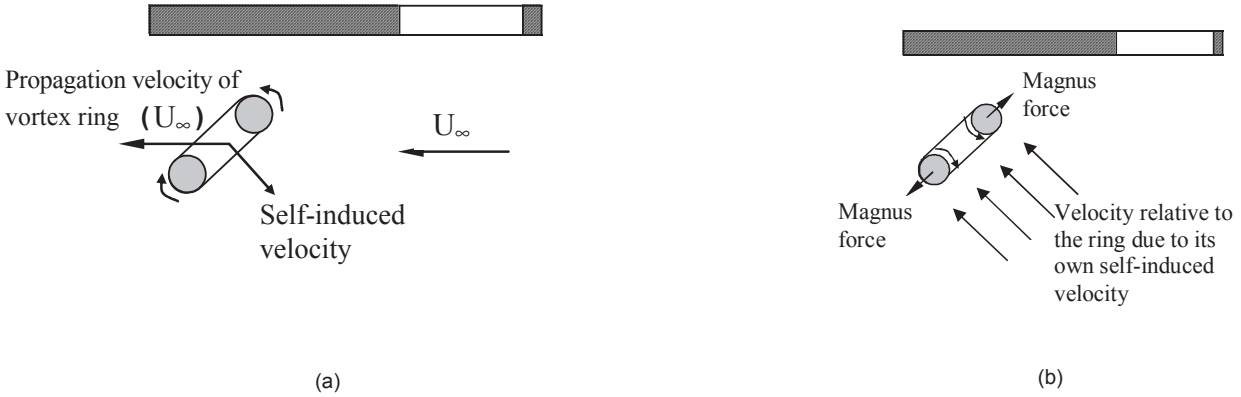


Figure 13. Vortex ring as it reaches its stable orientation (a) Its velocity components in a stationary co-ordinate;
(b) Flow velocity relative to the ring and the Magnus forces acting on the ring.

Chang and Vadili[16] suggested that the spinning solid cylinder model for a fluid vortex core with uniform vorticity proposed by Ting and Tung[17] could be used to explain qualitatively the tilting mechanism of vortex rings in a cross flow. However, a sufficient amount of description of this model has been not provided in either paper. In this paper, a model based on the spinning solid cylinder concept is illustrated in detail to explain the titling mechanism. The effect of shear is also discussed.

This model is explained as follows. When a vortex ring fully emerges from the orifice, it has a vertical velocity component U_y which is essentially the jet velocity and a very small streamwise velocity component U_x which can be approximated as zero (see Fig. 12(a)). The upstream and downstream part of this ring can be modeled as a pair of vortex rollers placed in a parallel stream. The velocity of this parallel stream U_r is the resultant velocity of U_y and the local velocity U in the boundary layer (see Fig. 12(b)). Due to its circulation, each roller will be subject to a Magnus force as illustrated in Fig. 12(b). The Magnus force produces a rotational moment around the centre of the vortex ring causing the ring to tilt in an anticlockwise direction. At the same time, there is a strong interaction between the vortex ring and the surrounding fluid flow such that the vortex ring accelerates in the streamwise direction and loses its initial momentum in the vertical direction. As a result, the magnitude of the Magnus force will reduce accordingly. Although vortex stretching may enhance tilting at some point, tilting will stop when the Magnus force that exerts on the upstream and downstream rollers lies in the plane of the ring (Fig. 13(b)). The whole process seems to occur within a streamwise distance of about ten orifice diameters. Further downstream, the vortex ring will remain at a constant inclination angle as it propagates with the main flow under the influence of its own self-induced velocity (Fig. 13(a)).

If the initial vertical velocity component of the vortex ring increases as a result of increasing diaphragm frequency and amplitude, the velocity vector of the flow relative to the ring U_r will turn towards the normal direction of the plane of the vortex ring. Consequently, the rotational moment produced by the Magnus force will decrease as the direction along which the Magnus forces act gradually turns towards the plane of the ring. Hence tilting will be less obvious at very high Reynolds numbers. This is evident in Fig. 6(f) and 6(i) where the vortex rings appear to be ejected through the boundary layer with less tilting. In addition, the amount of vortex stretching appears to be reduced too due to the very short time they are exposed to shear in the boundary layer.

The above model implies that vortex tilting is an inviscid phenomenon. Hence shear is not the cause for vortex tilting. There is evidence showing that tilting indeed occurs outside the boundary layer where shear is zero (see Fig. 6(f) and 6(i)). Nevertheless, tilting may be modulated by shear which alters the strength of circulation in the vortex ring and it may be enhanced by stretching which increases the rotational moment. It is also believed that although the onset of suction cycle can enhance tilting it is not necessary for tilting to occur since tilting is in fact a reaction of the ring to an initial large difference between the direction of flow velocity relative to the vortex ring and the normal direction of the ring.

https://doi.org/10.1017/S0001924000000877 Published online by Cambridge University Press

5.0 CONCLUSION

Dye flow visualisation of circular synthetic jets was undertaken in a laminar boundary layer developing over a flat plate at a range of actuator operating conditions and two freestream velocities. The purpose of this work was to study the interaction of synthetic jets with the boundary layer and the nature of vortical structures produced as a result of this interaction.

The effects of velocity ratio, Reynolds number and Strouhal number on the behaviour of synthetic jets were studied. Based on the experimental observations, the Reynolds number based on the stroke length is found to be adequate in quantifying the vorticity strength of the vortical structures. The velocity ratio, which indicates the relative strength between the jet and incoming flow in terms of velocity, appears to determine the trajectory of the structures as they propagate in the downstream. The Strouhal number mainly affects the spacing between consecutive structures. The combined effects of these parameters determine the structure of synthetic jets as they enter the boundary layer and their interaction with the layer.

At low Reynolds numbers and velocity ratios, the vortical structures generated by synthetic jets appear as highly stretched hairpin vortices which are attached to the wall. At intermediate Reynolds numbers and velocity ratios, the synthetic jets roll up into vortex rings which experience dramatic tilting and stretching as they enter the boundary layer. These vortex rings will eventually propagate outside the boundary layer hence the influence of the synthetic jets on the near wall flow will be confined in the near field of the orifice. At high Reynolds numbers and velocity ratios, the vortex rings appear to undergo a certain amount of tilting but no obvious stretching and they penetrate the edge of the boundary layer quickly, producing very limited impact on the near wall flow.

Based on the observations from the present experiment, it is believed that the hairpin vortices produced with relatively low jet Reynolds number and velocity ratios are likely to be responsible for producing the persistent streamwise vortex pairs that delayed flow separation. These hairpin vortices could be the desirable vortical structures for effective flow separation control which require minimal power consumptions. Further evidence confirming this conjecture will be sought by conducting detailed velocity measurements of synthetic jets in the boundary layer.

Finally, in this experiment vortex tilting and stretching are found to be the dominant features in the dynamics of vortical structures produced by synthetic jets. A vortex model was described which explains the mechanism of vortex tilting.

ACKNOWLEDGEMENT

This images presented in this paper were produced by the second author while he was an ERASMUS student from France doing his final year project at Manchester University in 2002. Helpful discussions with Mr Luis Garcillan regarding interpretation of the images are acknowledged.

REFERENCES

1. JAMES, R.D., JACOBS, J.W. and GLEZER, A. A round turbulent jet produced by an oscillating diaphragm, *Phys of Fluids,* 1996, **8,** (9), pp 2481-2495.
2. SMITH, B.L. and GLEZER, A. The formation and evolution of synthetic jets, *Phys of Fluids,* 1998, **10,** pp 2281-2297.
3. SEIFERT, A., BACHAR, T., KOSS, D., SHEPSHELOVICH, M. and WYGNANSKI, I. Oscillatory blowing: a tool to delay boundary-layer separation, *AIAA J,* 1993, **31,** (11).
4. MCMICHAEL, J.M. Progress and prospects for active flow control using microfabricated electro-mechanical systems (MEMS), AIAA paper 96-0306, 1996.
5. GAD-EL-HAK, M. Modern developments in flow control, *Applied Mech Rev,* 1996, **49,** (7), pp 365-379.
6. AMITAY, M., SMITH, B.L. and GLEZER, A. Aerodynamic flow control using synthetic jet technology, AIAA Paper 98-0208, 1998.
7. AMITAY, M., KINBENS, V., PAREKH, D. and GLEZER, A. The dynamics of flow reattachment over a thick airfoil controlled by synthetic jet actuators, AIAA Paper 99-1001, 1999.
8. CROOK, A. and WOOD, N.J. A parametric study of a synthetic jet in quiescent conditions, 9th International Symposium on Flow Visualisation, Paper 67, Edinburgh, UK, 2000.
9. CROOK, A., SADRI, A.M. and WOOD, N.J. The development and implementation of synthetic jets for the control of separated flow, AIAA paper 99-3176, 17th Applied Aerodynamics Conference, Norfolk, July 1999.
10. CROOK, A., CROWTHER, W.J. and WOOD, N.J. A parametric study of a synthetic jet in a cross flow, 22nd International Congress of Aeronautical Sciences, Harrogate, UK, 2000.
11. CROOK, A., CROWTHER, W.J. and WOOD, N.J. Measurements and visualisations of synthetic jets, AIAA paper 2001-0145, 39th Aerospace Sciences Meeting and Exhibit, Reno, Nevada, January 2001.
12. GLEZER, A. and AMITAY, M. Synthetic jets, *Annual Review Fluid Mech,* 2002, **34,** pp 503-529.
13. TANG, H. and ZHONG, S. Development of prediction models for synthetic jets in quiescent conditions using FLUENT, AIAA paper 2005-0104, The 43rd Aerospace Sciences Meeting and Exhibit, Reno, Nevada, USA, January 2005.
14. TANG, H. and ZHONG, S. 2D simulation of circular synthetic jets in quiescent conditions, *Aeronaut J,* 2005, **109**, (1092), pp 89-97.
15. HEAD, M.R. and BANDYOPADYAY, P. New aspects of turbulent boundary-layer structure, *J Fluid Mech,* 1981, **107,** pp 297-338.
16. CHANG, Y.K. and VAKILI, A.D. Dynamics of vortex rings in crossflow, *Physics of Fluids,* 1995, **7,** pp 1583-1597.
17. TING, L. and TUNG, C. Motion and decay of a vortex in a non-uniform stream, *Physics of Fluids,* 1965, **8,** p 1039.

https://doi.org/10.1017/S0001924000000877 Published online by Cambridge University Press